

# Self-Powered Solar-Blind Photodetector with Fast Response Based on Au/ $\beta$ -Ga<sub>2</sub>O<sub>3</sub> Nanowires Array Film Schottky Junction

Xing Chen,<sup>†</sup> Kewei Liu,<sup>\*,†</sup> Zhenzhong Zhang,<sup>†</sup> Chunrui Wang,<sup>‡</sup> Binghui Li,<sup>†</sup> Haifeng Zhao,<sup>†</sup> Dongxu Zhao,<sup>†</sup> and Dezhen Shen<sup>\*,†</sup>

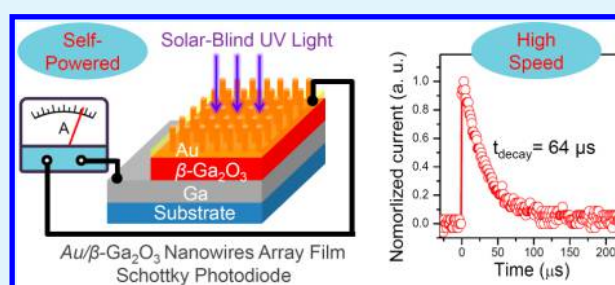
<sup>†</sup>State Key Laboratory of Luminescence and Applications and <sup>‡</sup>State Key Laboratory of Laser Interaction with Matter, Changchun Institute of Optics, Fine Mechanics and Physics, Chinese Academy of Sciences, 3888 Dongnanhu Road, Changchun 130033, PR China

## S Supporting Information

**ABSTRACT:** Because of the direct band gap of 4.9 eV,  $\beta$ -Ga<sub>2</sub>O<sub>3</sub> has been considered as an ideal material for solar-blind photodetection without any bandgap tuning. Practical applications of the photodetectors require fast response speed, high signal-to-noise ratio, low energy consumption and low fabrication cost. Unfortunately, most reported  $\beta$ -Ga<sub>2</sub>O<sub>3</sub>-based photodetectors usually possess a relatively long response time. In addition, the  $\beta$ -Ga<sub>2</sub>O<sub>3</sub> photodetectors based on bulk, the individual 1D nanostructure, and the film often suffer from the high cost, the low repeatability, and the relatively large dark current, respectively.

In this paper, a Au/ $\beta$ -Ga<sub>2</sub>O<sub>3</sub> nanowires array film vertical Schottky photodiode is successfully fabricated by a simple thermal partial oxidation process. The device exhibits a very low dark current of 10 pA at  $-30$  V with a sharp cutoff at 270 nm. More interestingly, the 90–10% decay time of our device is only around 64  $\mu$ s, which is much quicker than any other previously reported  $\beta$ -Ga<sub>2</sub>O<sub>3</sub>-based photodetectors. Besides, the self-powering, the excellent stability and the good reproducibility of Au/ $\beta$ -Ga<sub>2</sub>O<sub>3</sub> nanowires array film photodetector are helpful to its commercialization and practical applications.

**KEYWORDS:** solar-blind photodetector,  $\beta$ -Ga<sub>2</sub>O<sub>3</sub>, self-powered, high-speed, schottky junction



## 1. INTRODUCTION

Because of the strong absorption by stratospheric ozone, the ultraviolet radiation below 280 nm from the sun cannot penetrate the atmosphere to reach the earth's surface, which is thus called solar-blind region. If the photodetectors working in this region, the so-named solar-blind photodetectors, can detect a very weak signal under sun due to the absence of sky background interference. Therefore, the solar-blind photodetectors have many potential applications, such as missile alarming and tracking, high-pressure arc discharge detection, ozone monitoring and nonline-of-sight optical communication.<sup>1–5</sup>

Up to present, a number of solar-blind photodetectors have been demonstrated on wide bandgap semiconductors, including AlGa<sub>N</sub>,<sup>6–9</sup> MgZnO,<sup>4,10–13</sup> diamond,<sup>14–16</sup>  $\beta$ -Ga<sub>2</sub>O<sub>3</sub>,<sup>1,17–29</sup> and so on. Benefiting from the rapid development of their light emitting diode (LED) and related process technology,<sup>30</sup> AlGa<sub>N</sub>-based photodetectors present the more excellent performance than the other wide bandgap semiconductors devices. However, with increasing Al composition for solar-blind detection, the performance of AlGa<sub>N</sub> photodetectors rapidly becomes poor due to the obvious degradation of the crystal quality.<sup>6–9</sup> MgZnO alloys with a band gap in solar-blind region also suffer from the poor crystal quality due to the phase separation.<sup>4,10–13</sup> As for diamond, its band gap is as large as 5.5

eV, and thus its detection range is limited to shorter than 225 nm.<sup>16</sup>

$\beta$ -Ga<sub>2</sub>O<sub>3</sub>, with a direct band gap of 4.9 eV, is an ideal material for solar-blind photodetection without any bandgap tuning. It also possesses some unique advantages, such as large absorption coefficient ( $>10^5$  cm<sup>-1</sup> near band edge), high chemical and thermal stability.<sup>31</sup> In the past few years, a large number of solar-blind photodetectors have been demonstrated on  $\beta$ -Ga<sub>2</sub>O<sub>3</sub> with different phases, including bulk, thin films, and nanostructures.<sup>1,17–29</sup> As is well-known, practical applications of the photodetectors require fast response speed, high signal-to-noise ratio, low energy consumption and low fabrication cost.<sup>10,32</sup> According to the previous reports, the devices based on bulk and individual 1-D nanostructured  $\beta$ -Ga<sub>2</sub>O<sub>3</sub> usually show very high responsivity, but the high cost of bulk materials and the low repeatability of individual 1D nanostructure-based devices hinder their practical applications.<sup>19,24,26</sup> Although significant progress has been made in the epitaxial growth of  $\beta$ -Ga<sub>2</sub>O<sub>3</sub> thin films, their solar-blind photodetectors usually have a relatively higher dark current and a slower response speed.<sup>21–23</sup> Recently, it is found that the nanofilm photodetectors have obvious merits over other

Received: December 8, 2015

Accepted: January 28, 2016

Published: January 28, 2016

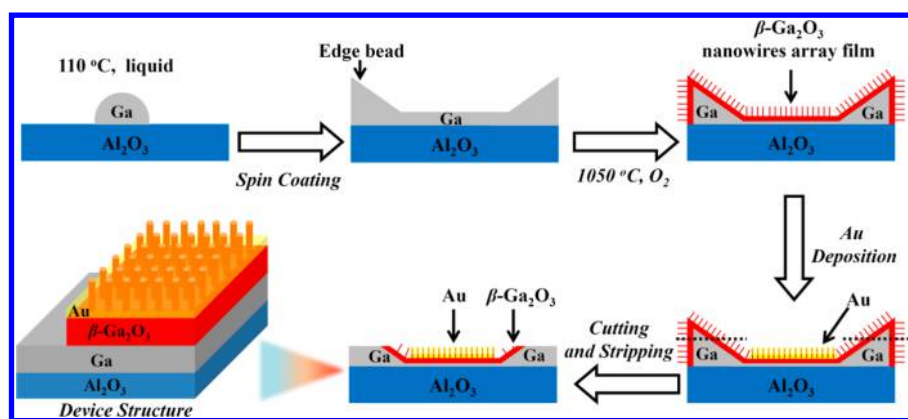


**Figure 1.** Schematic illustration of the fabrication of  $\beta$ -Ga<sub>2</sub>O<sub>3</sub> nanowires array film and its vertical Schottky photodiode.

devices based on bulk, thin films, and 1D nanostructures, such as easy fabrication, low cost, flexible, and high performance.<sup>33</sup> Until now, many solar-blind photodetectors have been demonstrated on  $\beta$ -Ga<sub>2</sub>O<sub>3</sub> nanostructured films.<sup>28,29</sup> However, all these devices have simple metal–semiconductor–metal (MSM) structure and their performance is thus still worse than expected. Considering the potential applications in secure communication and space detection, the quick response speed and the self-powered ability for a solar-blind photodetector are strongly desirable. Therefore, the vertical Schottky photodiode based on  $\beta$ -Ga<sub>2</sub>O<sub>3</sub> nanostructured films should satisfy this requirement. Unfortunately, no information regarding this can be found.

As is well-known, a vertical Schottky photodiode usually consist of three parts: an Ohmic contact electrode at the bottom, a semiconductor sensitive layer, and a Schottky contact electrode on the top. Two types of electrodes at the different position make the devices fabrication process complex. In this paper, a vertical Schottky photodiode based on  $\beta$ -Ga<sub>2</sub>O<sub>3</sub> nanostructured film was fabricated by a simple method. By partial oxidation of Ga metal at high temperature,  $\beta$ -Ga<sub>2</sub>O<sub>3</sub> nanowires array films can be formed on the surface. At the same time, a good Ohmic contact was established between the residual Ga and  $\beta$ -Ga<sub>2</sub>O<sub>3</sub> nanowires array film. After the deposition of a 20 nm Au layer as the Schottky electrode, a vertical Schottky photodiode was demonstrated. A sharp cutoff wavelength at around 270 nm, and a liner relationship between photocurrent and light intensity ( $\lambda = 254$  nm) can be clearly observed. More interestingly, the 90–10% decay time of our device is only  $\sim 64$   $\mu$ s, which is much quicker than any other  $\beta$ -Ga<sub>2</sub>O<sub>3</sub>-based photodetectors reported previously. In addition, this  $\beta$ -Ga<sub>2</sub>O<sub>3</sub> nanowires array film shows an obvious solar-blind response without any power supply. Our findings indicated that this simple partial oxidation method can be used to fabricate self-powered solar-blind photodetectors with fast response speed for the potential applications insecure communication and space detection.

## 2. EXPERIMENTAL SECTION

**2.1. Synthesis and Characterization of the  $\beta$ -Ga<sub>2</sub>O<sub>3</sub> Nanowires Array Film.** The  $\beta$ -Ga<sub>2</sub>O<sub>3</sub> nanowires array film was synthesized by partial thermal oxidation process. First, the liquid metal Ga (20 mg, 110 °C) was coating on the surface of *c*-sapphire substrate ( $8 \times 8$  mm<sup>2</sup>). Then the substrate was rotated by the spin coater and the typically rotate speed is 7500 rpm for 20 s. Due to the spin coating process, the Ga edge bead was formed on the edge of the *c*-sapphire substrate. Then, the Ga/*c*-sapphire was placed in a horizontal tube

furnace at 1050 °C for 60 min with a flow of highly pure oxygen. First, the top surface of Ga was oxidation to form the  $\beta$ -Ga<sub>2</sub>O<sub>3</sub>. After that, the  $\beta$ -Ga<sub>2</sub>O<sub>3</sub> layer can protect the interior of the Ga to avoid further oxidation. In addition, the  $\beta$ -Ga<sub>2</sub>O<sub>3</sub> nanowires were formed on the  $\beta$ -Ga<sub>2</sub>O<sub>3</sub> layer during the oxidation process. The samples were characterized by using scanning electron microscopy (SEM) (HITACHI S-4800), energy dispersive X-ray spectrometry (EDS) (GENESIS 2000 XMS60S), Bruker D8GADDS, X-ray diffraction (XRD) using Cu *K* $\alpha$  radiation ( $\lambda = 0.154$  nm) with an area detector, transmission electron microscopy (TEM), high resolution transmission electron microscopy (HRTEM), and selected area electron diffraction (SAED) (JEOL JEM-2100F electron microscope).

### 2.2. Fabrication and Characterization of the Photodiode.

A 20 nm-thick Au layer was deposited on the surface of the  $\beta$ -Ga<sub>2</sub>O<sub>3</sub> through a mask, and a vertical Schottky photodiode was thus demonstrated with Au as Schottky contact electrode and Ga as Ohmic contact electrode. The SEM image of the  $\beta$ -Ga<sub>2</sub>O<sub>3</sub> nanowires coated by Au was shown in Figure S1 in the Supporting Information. The current–voltage (*I*–*V*) properties were measured by using a semiconductor device analyzer (Agilent B1500A). A 200 W UV-enhanced Xe lamp with a monochromator was used to investigate the spectral response properties of the photodetectors. The transient response spectra of photodetectors were recorded by using an oscilloscope (Tektronix DPO 5104 digital oscilloscope) and a Nd:YAG laser (266 nm).

## 3. RESULTS AND DISCUSSION

Figure 1 shows the schematic illustration of the fabrication of  $\beta$ -Ga<sub>2</sub>O<sub>3</sub> nanowires array film and its vertical Schottky photodiode. First, the liquid Ga metal was spin-coated on a *c*-face sapphire, and then a thin Ga layer was formed with an edge bead. After thermal oxidation at 1050 °C in oxygen,  $\beta$ -Ga<sub>2</sub>O<sub>3</sub> nanowires array film can be prepared on the Ga metal surface. Then the  $\beta$ -Ga<sub>2</sub>O<sub>3</sub> layer can protect the interior of the Ga to avoid further oxidation, and thus a thin Ga metal layer would remain between  $\beta$ -Ga<sub>2</sub>O<sub>3</sub> and substrate, which can be used as Ohmic electrode. After that, a 20 nm-thick Au layer was deposited on the surface of the  $\beta$ -Ga<sub>2</sub>O<sub>3</sub> through a mask as Schottky electrode. According to the SEM and EDS mapping results (see figures S1 and S2 in the Supporting Information), Au is deposited on the surface of both  $\beta$ -Ga<sub>2</sub>O<sub>3</sub> layer and  $\beta$ -Ga<sub>2</sub>O<sub>3</sub> nanowires. After cutting and stripping, a vertical Schottky photodiode with a Au Schottky contact and a Ga Ohmic contact was demonstrated based on  $\beta$ -Ga<sub>2</sub>O<sub>3</sub> nanowires array film. In Figure 2, a cross-sectional SEM image of the sample is shown, and an EDS line scan is taken along the white dashed line. The spatial distributions of O, Ga and Al indicated that the sample has a trilayer structure, namely,  $\beta$ -Ga<sub>2</sub>O<sub>3</sub> nanowires array/ $\beta$ -Ga<sub>2</sub>O<sub>3</sub> film/Ga. The thickness of the

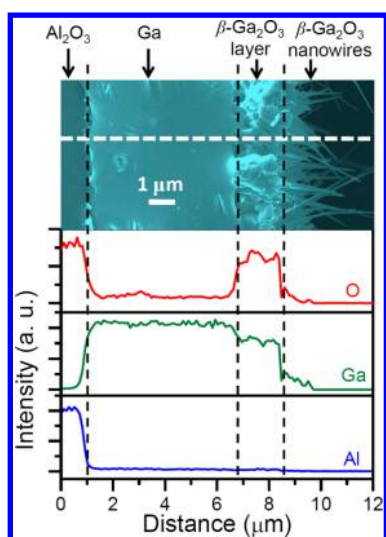


**Figure 2.** Cross-sectional SEM image of the sample and line scanning EDS on the cross-sectional of the sample along the white dashed line.

residual Ga layer and  $\beta\text{-Ga}_2\text{O}_3$  layer is approximately 5.8 and 1.6  $\mu\text{m}$ , respectively.

To investigate further the crystal structure of  $\beta\text{-Ga}_2\text{O}_3$  nanowires array film, SEM, XRD, and TEM measurements were carried out. Figure 3a presents the SEM image of  $\beta\text{-Ga}_2\text{O}_3$  nanowires array film. It can be found that most  $\beta\text{-Ga}_2\text{O}_3$  nanowires are perpendicular to the substrate, and their average length and diameter is around 1–3  $\mu\text{m}$  and 100–200 nm, respectively. The XRD pattern of the sample is shown in Figure 3b. Besides the diffraction of the *c*-sapphire substrate, all other diffraction peaks can be indexed to the monoclinic  $\beta\text{-Ga}_2\text{O}_3$  with lattice parameters  $a = 1.223$  nm,  $b = 0.304$  nm,  $c = 0.580$  nm, and  $\beta = 103.7^\circ$  (JCPDS Card No. 43-1012). Among them, three strong diffraction peaks located at  $18.9^\circ$ ,  $38.4^\circ$ , and  $59.2^\circ$  could be assigned as  $(-201)$ ,  $(-402)$ , and  $(-603)$  planes of  $\beta\text{-Ga}_2\text{O}_3$ , respectively. The diffraction peaks of Ga do not appear due to the liquid nature of Ga metal (melt point:  $29.8^\circ\text{C}$ ) in our sample. Because of the absolute quantity of  $\beta\text{-Ga}_2\text{O}_3$  layer should be much larger than that of nanowires (see Figure 2), the signal from the layer should be much stronger compared to that of the nanowires in the XRD pattern. Thus, from the XRD result, we can only confirm that the underlayer of our

nanowires array film is  $\beta\text{-Ga}_2\text{O}_3$ . As for the crystal structure of the nanowires, Figure 3c,d presents the low- and high-resolution TEM images of the individual nanowire scraped from the  $\beta\text{-Ga}_2\text{O}_3$  nanowires array film. The lattice fringes with a  $d$ -spacing of 0.2667 nm were observed, which correspond to the  $(11\bar{1})$  lattice planes of  $\beta\text{-Ga}_2\text{O}_3$ . Figure 3e shows the SAED pattern of the nanowire, which can be indexed to  $[1\bar{1}0]$  zone axis of  $\beta\text{-Ga}_2\text{O}_3$ , indicating the single crystalline nature of this nanowire. The TEM images and SAED pattern results indicate that the nanowires have the same monoclinic structure with  $\beta\text{-Ga}_2\text{O}_3$  layer and are grown along the  $[110]$  direction.

To investigate the optoelectronic properties of  $\beta\text{-Ga}_2\text{O}_3$  nanowires array film, the vertical Schottky photodetector has been fabricated on this film. Figure 4 shows the  $I$ – $V$

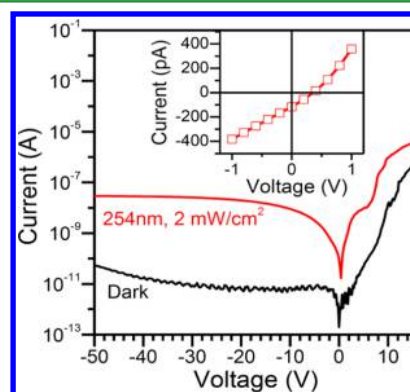


**Figure 4.**  $I$ – $V$  characteristics of device in dark and under the illumination of 254 nm light in the logarithmic scale. Inset shows the photovoltaic characteristic of the device near zero bias.

characteristics of device both in the dark and under 254 nm light illumination ( $2\text{ mW}/\text{cm}^2$ ) at the room temperature. The photodiode exhibits a good rectifying property under dark condition with a current rectification ratio of  $10^5$  at  $\pm 15$  V and a turn-on voltage of  $\sim 10$  V. The leakage current is as low as  $\sim 10$  pA at the reverse bias of 30 V. In addition, the device reveals a high breakdown voltage of over  $-50$  V. Moreover, the  $I$ – $V$  characteristics of the Schottky junction can be described by thermionic emission theory, and the current across a Schottky barrier ( $I$ ) can be expressed as<sup>34</sup>

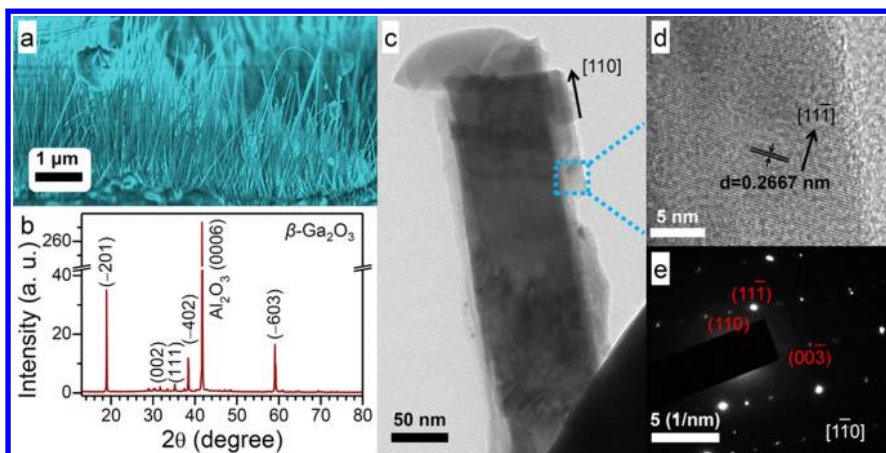


**Figure 3.** (a) SEM image and (b) XRD pattern of the  $\beta\text{-Ga}_2\text{O}_3$  nanowires array film. (c) Low- and (d) high-resolution TEM images of the  $\beta\text{-Ga}_2\text{O}_3$  nanowire. (e) SAED pattern along  $[1\bar{1}0]$  zone axis.

$$I = I_S [e^{q(V-R_S I)/nk_B T} - 1] \quad (1)$$

where  $q$  is the electron charge,  $R_S$  is the series resistance,  $n$  is the ideality factor,  $k_B$  is the Boltzmann factor,  $T$  is the operating temperature, and  $I_S$  is the saturation current. By fitting the experimental data of our Au/ $\beta$ -Ga<sub>2</sub>O<sub>3</sub> nanowires array film Schottky photodiode using eq 1,  $n$  and  $R_S$  could be estimated to be  $\sim 30$  and  $\sim 10^8 \Omega$ , respectively. According to the previous reports, this large  $n$  can be attributed to damage or insulating interfacial layer between Au electrode and  $\beta$ -Ga<sub>2</sub>O<sub>3</sub> semiconductor<sup>35,36</sup>. The inset of Figure 4 shows the photovoltaic characteristic of the device near zero bias, and a typical photovoltaic effect could be observed clearly. The open-circuit photovoltage and the short circuit current can be deduced to be 0.36 V and 120 pA, respectively, and this characteristic of the device shows a good reproducibility (see Figure S3 in the Supporting Information). This result suggests that our Au/ $\beta$ -Ga<sub>2</sub>O<sub>3</sub> nanowires array film Schottky photodiode can be operated without any external power supply, namely it is a self-powered device.

Figure 5 shows the spectral responses of the Au/ $\beta$ -Ga<sub>2</sub>O<sub>3</sub> nanowires array film Schottky photodiode at zero bias and

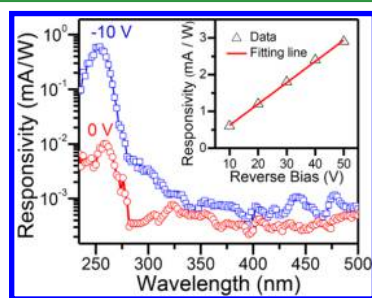


**Figure 5.** Spectral responses of the device at zero bias and under reverse bias of 10 V. Inset shows the responsivity of photodetectors at the wavelength of 254 nm as a function of reverse bias.

under reverse bias of 10 V. Obviously, the device displayed true solar-blind photoresponse with a cutoff wavelength of  $\sim 270$  nm both at 0 V and reverse 10 V. As shown in Figure 5, the device shows nearly no response under the illumination with a wavelength longer than 310 nm. When the wavelength is shorter than 280 nm, the responsivity increases sharply with the decrease of light wavelength and reaches its peak value at  $\sim 258$  nm, corresponding to the absorption edge of  $\beta$ -Ga<sub>2</sub>O<sub>3</sub>. This phenomenon indicates that the photogenerated electron–hole pairs are mainly excited by the light with the energy larger than the bandgap of  $\beta$ -Ga<sub>2</sub>O<sub>3</sub>. At 0 V bias, the peak responsivity is around 0.01 mA/W, and a solar-blind/UV rejection ratio ( $R_{258 \text{ nm}}/R_{280 \text{ nm}}$ ) of  $\sim 11$  and a UV/visible rejection ratio ( $R_{258 \text{ nm}}/R_{400 \text{ nm}}$ ) of  $\sim 38$  are obtained. When the photodiode is operated at a reverse bias of 10 V, the peak responsivity can reach 0.6 mA/W, and its solar-blind/UV rejection ratio and UV/visible rejection ratio are around  $1 \times 10^2$  and  $2 \times 10^3$ , respectively. The inset of Figure 5 shows the peak responsivity of photodetector as a function of reverse bias. With increasing the reverse bias from 0 to 50 V, the responsivity increases linearly. A responsivity of 2.9 mA/W can be obtained under the reverse bias of 50 V.

One key parameter for a photodetector is the response speed, which determines its capability to follow a fast-varying optical signal. According to the previous reports, the response time (both rise and fall time) of the  $\beta$ -Ga<sub>2</sub>O<sub>3</sub> based

photodetectors is usually in seconds.<sup>23,26,27,29</sup> And this slow response speed limits the practical applications of the devices. Interestingly, our Au/ $\beta$ -Ga<sub>2</sub>O<sub>3</sub> nanowires array film Schottky photodiode presents relatively quick response to the solar-blind UV light. Figure 6a shows the schematic diagram of the experimental setup for the measurement of response time. The temporal response of the device was analyzed by a pulsed Nd:YAG laser with a 266 nm wavelength (the laser pulse width was 10 ns and the frequency was 10 Hz). A Tektronix DPO 5104 digital oscilloscope was used to monitor the time dependence of the photocurrent. In Figure 6b, a good reproducibility and stability of our device can be clearly observed and the response speed is very fast. The 10–90% rise time (defined as the time for the current increasing from 10% to 90% of the peak value) of the device is around 1  $\mu$ s (see Figure 6c). In addition, the 90–10% decay time (defined as the time for the current dropping from 90% to 10% of the peak value) of the device is around 64  $\mu$ s, and the current drops to zero at about 100  $\mu$ s. As far as we know, the response speed of our device is by far the quickest one among the various  $\beta$ -Ga<sub>2</sub>O<sub>3</sub> photodetectors. In order to further understand the decay process, we fit the decreasing portion of the temporal response with an exponential decay curve, and a good fit was accomplished using a first-order exponential decay with time constants of 31  $\mu$ s. The RC constant may be responsible for the slow decay component, where  $R$  is the total resistance and  $C$  is mainly the capacitance of the depletion layer in the photodiode. The detector capacitance was estimated to be  $\sim 0.54$  pF by the actual capacitance–voltage ( $C$ – $V$ ) measurement (see Figure S4 in the Supporting Information), and the RC time constant is around 54  $\mu$ s (assuming  $R \approx R_S = 10^8 \Omega$ ). This value of RC time constant is on the same order as our fitting result as shown in Figure 6c, and thus the relatively slow decay process can be mainly attributed to the RC time constant. Besides, the long lifetime of the photoexcited carriers in the  $\beta$ -Ga<sub>2</sub>O<sub>3</sub> induced by carrier trapping effect cannot be completely ruled out in this work. In Figure 6d, the decay time at different reverse bias was shown. With increasing the reverse bias, the decay time only changes a little. This phenomenon can be explained as follows: due to the very low carrier concentration ( $\sim 10^{14} \text{ cm}^{-3}$ ), the entire  $\beta$ -Ga<sub>2</sub>O<sub>3</sub> layer would be depleted even at a small reverse bias. As a result, when we increase the reverse bias, the change of the device capacitance should be very small, which is further confirmed by the actual  $C$ – $V$  measurement as shown in Figure S4. The RC constant is thus almost no change, resulting in the independence of the decay time on the reverse bias. In addition, the response speed is also measured using a lamp ( $\lambda = 254$  nm) modulated by a mechanical chopper (see Figure S5 in the Supporting Information). With increasing the frequency from 15 to 120 Hz ( $16 \text{ mW/cm}^2$ ), the decay time decreases from  $\sim 10$  to  $\sim 3$  ms. However, with the decrease of the light intensity from 16 to 4  $\text{mW/cm}^2$  at 60 Hz, the change of the decay time is very small ( $\sim 5$  ms). Notably, the decay time measured using the chopped lamp is much longer than that measured using a pulsed laser, and this slow decay should be determined by the excitation profile of the mechanically chopped lamp.

Figure 7a shows the time-dependent response of the Au/ $\beta$ -Ga<sub>2</sub>O<sub>3</sub> nanowires array film Schottky photodiode, which is measured by periodically turning on and off a 254 nm light at a bias of 0 V. Upon the 254 nm light illumination ( $2 \text{ mW}\cdot\text{cm}^{-2}$ ), the current instantaneously increased to 0.15 nA. After turning off the light, the current quickly returned to its original value. The time-dependent response to the light on/off cycles shows

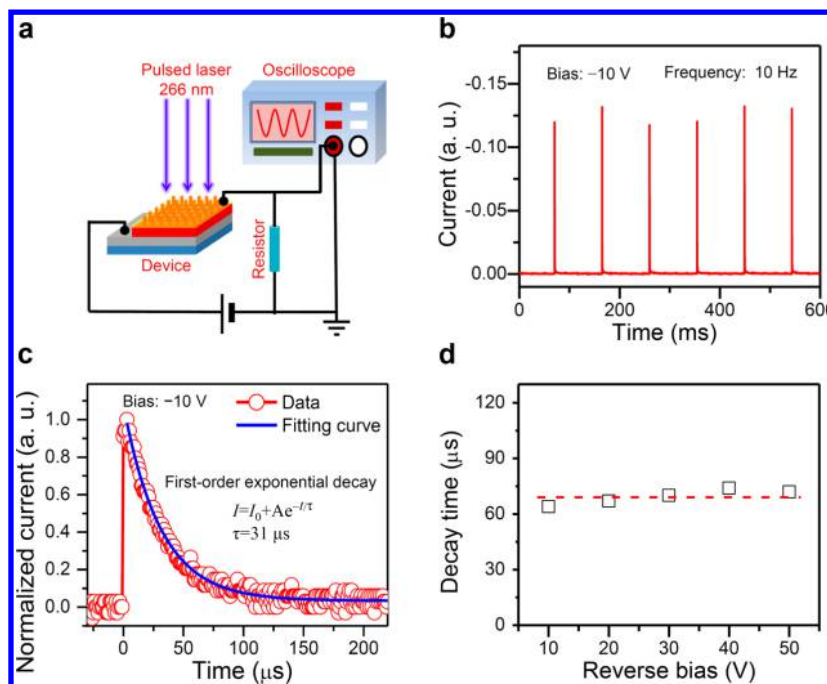


**Figure 6.** (a) Schematic diagram of our experimental setup for measuring the time response of the photodetectors. (b) Time-resolved response of the photocurrent of  $\beta$ -Ga<sub>2</sub>O<sub>3</sub> nanowires array film/Au Schottky photodiode at  $-10$  V under illumination of a Nd:YAG laser with a wavelength of 266 nm and a frequency of 10 Hz. (c) Decay edge of the current response at reverse bias of 10 V. (d) Decay time of the photodiode under different reverse bias.

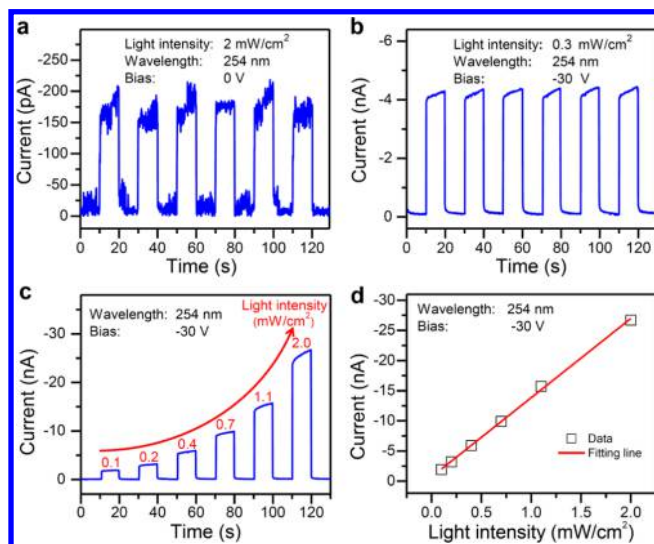


**Figure 7.** Time-dependent photocurrent response of Au/ $\beta$ -Ga<sub>2</sub>O<sub>3</sub> nanowires array film Schottky photodiode measured at the different conditions: (a) illuminated by 254 nm light with the intensity of 2 mW·cm<sup>-2</sup> at 0 V, (b) illuminated by 254 nm light with the intensity of 0.3 mW·cm<sup>-2</sup> at  $-30$  V, (c) illuminated by 254 nm light with various light intensities at  $-30$  V. (d) Photocurrent as a function of light intensity.

good stability and reproducibility. The similar phenomenon was also observed under bias of reverse 30 V with the light intensity of 0.3 mW·cm<sup>-2</sup> (see Figure 7b). To investigate further the ability of the device to respond to the intensity of the light, 254 nm light with the intensities ranging from 0.1 to 2.0 mW·cm<sup>-2</sup> was irradiated on the Au/ $\beta$ -Ga<sub>2</sub>O<sub>3</sub> nanowires array film Schottky photodiode at  $-30$  V as shown in Figure 7c. With increasing the light intensity, the device shows a

corresponding response. Figure 7d presents the photocurrent as a function of light intensity. Obviously, the photocurrent increases linearly with the increase of light intensity from 0.1 to 2.0 mW·cm<sup>-2</sup>. This nearly linear relationship between the photocurrent and excitation power intensity suggests that our devices can be used to measure solar-blind ultraviolet quantitatively.

The Au/ $\beta$ -Ga<sub>2</sub>O<sub>3</sub> nanowires array film Schottky photodiode shows a good performance in the solar-blind UV detection. And the novel fabrication process and device structure should play a fundamental role in our case. Table 1 shows a comparison of the photoresponse parameters for the  $\beta$ -Ga<sub>2</sub>O<sub>3</sub>-based photodetectors. It can be seen from the table that our Au/ $\beta$ -Ga<sub>2</sub>O<sub>3</sub> nanowires array film Schottky photodiode has the quickest rise and decay time. Moreover, the dark current of our device is lower than that of most other devices reported previously. The nature of the Schottky junction allows our device to be operated without any power supply. Although the performance of the Au/ $\beta$ -Ga<sub>2</sub>O<sub>3</sub> nanowires array film Schottky photodiode is still lower than the expected, we can improve it by optimizing device technology and structure, controlling the defects in semiconductor,<sup>34,37,38</sup> and using the surface plasmon effect and so on.<sup>39–41</sup> Our findings in this work suggest a possible method to realize the self-powered solar-blind photodetector with fast response speed.

#### 4. CONCLUSIONS

We have demonstrated a self-powered solar-blind photodetector based on Au/ $\beta$ -Ga<sub>2</sub>O<sub>3</sub> nanowires array film Schottky junction by a simple partial thermal oxidation process. Interestingly, during the partial oxidation of Ga to form  $\beta$ -Ga<sub>2</sub>O<sub>3</sub> nanowires array film, a good Ohmic contact can be easily achieved between them. The Au/ $\beta$ -Ga<sub>2</sub>O<sub>3</sub> nanowires array film Schottky photodiode exhibits a good rectifying

Table 1. Comparison of the Photoresponse Parameters Between the  $\beta$ -Ga<sub>2</sub>O<sub>3</sub> based Photodetectors

structure of $\beta$ -Ga <sub>2</sub> O <sub>3</sub>	structure of device	rise time/decay time (s)	dark current (pA)	responsivity (mA/W)	self-powered	ref
film	MSM		1200 (10 V)	37 (10 V)	no	18
film	MSM		620 (20 V)	1700 (20 V)	no	21
film	MSM	~1/~1	$1.28 \times 10^5$ (10 V)		no	23
single crystal	Schottky		$1 \times 10^4$ (-10 V)	8700 (-10 V)	yes	19
single crystal	Schottky		1000 (-3 V)	$1 \times 10^6$ (-3 V)	yes	24
bridged 1-D nanostructure	MSM	-/0.02	0.2 (50 V)		no	1
individual 1-D nanostructure	MSM	1/0.6	0.1 (6 V)	$5.47 \times 10^5$ (6 V)	no	26
multilayer 1-D nanostructure	MSM	0.3/0.3	0.1 (20 V)	$8.5 \times 10^5$ (20 V)	no	27
nanostructure film	MSM		133 (5 V)	0.37 (5 V)	no	28
nanostructure film	MSM	~40/~100	5000 (20 V)		no	29
nanostructure film	Schottky	$\sim 1 \times 10^{-6}/\sim 6 \times 10^{-5}$	10 (-30 V)	0.01 (0 V) 2.9 (-50 V)	yes	this work

property, and its dark current is only 10 pA at -30 V. Further photoresponse analysis showed that our device is a true solar-blind photodetector with a cutoff edge at  $\sim 270$  nm and can be operated under zero bias (photovoltaic mode). Moreover, the rise and decay time of the device is only  $\sim 1$  and  $64 \mu\text{s}$ , respectively, which is much shorter than any other previously reported  $\beta$ -Ga<sub>2</sub>O<sub>3</sub> based photodetectors. And the relatively slow decay process should be limited by the RC constant. Besides, the photodetector performs with excellent stability and reproducibility. Our findings suggest the great application potential of Au/ $\beta$ -Ga<sub>2</sub>O<sub>3</sub> nanowires array film Schottky photodetector in high-speed secure communication, space detection, missile alarming and tracking and so on.

## ■ ASSOCIATED CONTENT

### ■ Supporting Information

The Supporting Information is available free of charge on the ACS Publications website at DOI: 10.1021/acsami.5b11956.

Figure S1. SEM image of the  $\beta$ -Ga<sub>2</sub>O<sub>3</sub> nanowires coated by Au. Figure S2. (a) Cross-sectional SEM image of the Au/ $\beta$ -Ga<sub>2</sub>O<sub>3</sub> nanowires array film heterojunction. (b, c, and d) are the EDS mapping images of Ga, Au, and O, respectively. Figure S3. The repeated measurement of the  $I$ - $V$  characteristics of device under 254 nm light illumination ( $2 \text{ mW}/\text{cm}^2$ ). Figure S4:  $C$ - $V$  curve of the device. Figure S5. Time-resolved response of the photocurrent of the device at -40 V under the illumination of a 254 nm lamp (modulated by a mechanical chopper) with different (a) chopper frequencies and (b) light intensities (PDF).

## ■ AUTHOR INFORMATION

### ■ Corresponding Authors

\*K. Liu. E-mail: liukw@ciomp.ac.cn.

\*D. Shen. E-mail: shendz@ciomp.ac.cn.

### ■ Author Contributions

The paper was written through contributions of all authors. All authors have given approval to the final version of the paper.

### ■ Notes

The authors declare no competing financial interest.

## ■ ACKNOWLEDGMENTS

This work is supported by National Natural Science Foundation of China (Nos. 61475153, 10974197, 11174273, 11104265, 11134009, 61177040, 61376054), and the 100 Talents Program of the Chinese Academy of Sciences.

## ■ REFERENCES

- (1) Li, Y. B.; Tokizono, T.; Liao, M. Y.; Zhong, M. A.; Koide, Y.; Yamada, I.; Delaunay, J. J. Efficient Assembly of Bridged Beta-Ga<sub>2</sub>O<sub>3</sub> Nanowires for Solar-Blind Photodetection. *Adv. Funct. Mater.* **2010**, *20*, 3972–3978.
- (2) Han, S.; Zhang, J. Y.; Zhang, Z. Z.; Zhao, Y. M.; Wang, L. K.; Zheng, J. A.; Yao, B.; Zhao, D. X.; Shen, D. Z. Mg<sub>0.58</sub>Zn<sub>0.42</sub>O Thin Films on MgO Substrates with MgO Buffer Layer. *ACS Appl. Mater. Interfaces* **2010**, *2*, 1918–1921.
- (3) Liu, K. W.; Sakurai, M.; Aono, M.; Shen, D. Z. Ultrahigh-Gain Single SnO<sub>2</sub> Microrod Photoconductor on Flexible Substrate with Fast Recovery Speed. *Adv. Funct. Mater.* **2015**, *25*, 3157–3163.
- (4) Fan, M. M.; Liu, K. W.; Zhang, Z. Z.; Li, B. H.; Chen, X.; Zhao, D. X.; Shan, C. X.; Shen, D. Z. High-Performance Solar-Blind Ultraviolet Photodetector Based on Mixed-Phase ZnMgO Thin Film. *Appl. Phys. Lett.* **2014**, *105*, 011117-1–011117-5.
- (5) Su, L. X.; Zhu, Y.; Yong, D. Y.; Chen, M. M.; Ji, X.; Su, Y. Q.; Gui, X. C.; Pan, B. C.; Xiang, R.; Tang, Z. K. Wide Range Bandgap Modulation Based on ZnO-based Alloys and Fabrication of Solar Blind UV Detectors with High Rejection Ratio. *ACS Appl. Mater. Interfaces* **2014**, *6*, 14152–14158.
- (6) Walker, D.; Kumar, V.; Mi, K.; Sandvik, P.; Kung, P.; Zhang, X. H.; Razezghi, M. Solar-Blind AlGaIn Photodiodes With Very Low Cutoff Wavelength. *Appl. Phys. Lett.* **2000**, *76*, 403–405.
- (7) Cicek, E.; McClintock, R.; Cho, C. Y.; Rahnema, B.; Razezghi, M. Al<sub>x</sub>Ga<sub>1-x</sub>N-Based Back-Illuminated Solar-Blind Photodetectors with External Quantum Efficiency of 89%. *Appl. Phys. Lett.* **2013**, *103*, 191108-1–191108-4.
- (8) Parish, G.; Keller, S.; Kozodoy, P.; Ibbetson, J. P.; Marchand, H.; Fini, P. T.; Fleischer, S. B.; DenBaars, S. P.; Mishra, U. K.; Tarsa, E. J. High-Performance (Al, Ga)N-Based Solar-Blind Ultraviolet p-i-n Detectors on Laterally Epitaxially Overgrown GaN. *Appl. Phys. Lett.* **1999**, *75*, 247–249.
- (9) Biyikli, N.; Kimukin, I.; Aytur, O.; Ozbay, E. Solar-Blind AlGaIn-Based p-i-n Photodiodes with Low Dark Current and High Detectivity. *IEEE Photonics Technol. Lett.* **2004**, *16*, 1718–1720.
- (10) Liu, K. W.; Sakurai, M.; Aono, M. ZnO-Based Ultraviolet Photodetectors. *Sensors* **2010**, *10*, 8604–8634.
- (11) Wang, L. K.; Ju, Z. G.; Zhang, J. Y.; Zheng, J.; Shen, D. Z.; Yao, B.; Zhao, D. X.; Zhang, Z. Z.; Li, B. H.; Shan, C. X. Single-Crystalline Cubic MgZnO Films and Their Application in Deep-Ultraviolet Optoelectronic Devices. *Appl. Phys. Lett.* **2009**, *95*, 131113-1–131113-3.
- (12) Du, X. L.; Mei, Z. X.; Liu, Z. L.; Guo, Y.; Zhang, T. C.; Hou, Y. N.; Zhang, Z.; Xue, Q. K.; Kuznetsov, A. Y. Controlled Growth of High-Quality ZnO-Based Films and Fabrication of Visible-Blind and Solar-Blind Ultra-Violet Detectors. *Adv. Mater.* **2009**, *21*, 4625–4630.
- (13) Fan, M. M.; Liu, K. W.; Chen, X.; Wang, X.; Zhang, Z. Z.; Li, B. H.; Shen, D. Z. Mechanism of Excellent Photoelectric Characteristics in Mixed-Phase ZnMgO Ultraviolet Photodetectors with Single Cutoff Wavelength. *ACS Appl. Mater. Interfaces* **2015**, *7*, 20600–20606.

- (14) Foulon, F.; Bergonzo, P.; Borel, C.; Marshall, R. D.; Jany, C.; Besombes, L.; Brambilla, A.; Riedel, D.; Miseur, L.; Castex, M. C.; Gicquel, A. Solar Blind Chemically Vapor Deposited Diamond Detectors For Vacuum Ultraviolet Pulsed Light-Source Characterization. *J. Appl. Phys.* **1998**, *84*, 5331–5336.
- (15) Koide, Y.; Liao, M. Y.; Alvarez, J. Thermally Stable Solar-Blind Diamond UV Photodetector. *Diamond Relat. Mater.* **2006**, *15*, 1962–1966.
- (16) Gorokhov, E. V.; Magunov, A. N.; Feshchenko, V. S.; Altukhov, A. A. Solar-Blind UV Flame Detector Based on Natural Diamond. *Instrum. Exp. Tech.* **2008**, *51*, 280–283.
- (17) Kokubun, Y.; Miura, K.; Endo, F.; Nakagomi, S. Sol-Gel Prepared Beta-Ga<sub>2</sub>O<sub>3</sub> Thin Films for Ultraviolet Photodetectors. *Appl. Phys. Lett.* **2007**, *90*, 031912-1–031912-3.
- (18) Oshima, T.; Okuno, T.; Fujita, S. Ga<sub>2</sub>O<sub>3</sub> Thin Film Growth on c-Plane Sapphire Substrates by Molecular Beam Epitaxy for Deep-Ultraviolet Photodetectors. *Jpn. J. Appl. Phys.* **2007**, *46*, 7217–7220.
- (19) Oshima, T.; Okuno, T.; Arai, N.; Suzuki, N.; Ohira, S.; Fujita, S. Vertical Solar-Blind Deep-Ultraviolet Schottky Photodetectors Based on Beta-Ga<sub>2</sub>O<sub>3</sub> Substrates. *Appl. Phys. Express* **2008**, *1*, 011202-1–011202-3.
- (20) Li, L.; Auer, E.; Liao, M. Y.; Fang, X. S.; Zhai, T. Y.; Gautam, U. K.; Lugstein, A.; Koide, Y.; Bando, Y.; Golberg, D. Deep-Ultraviolet Solar-Blind Photoconductivity of Individual Gallium Oxide Nanobelts. *Nanoscale* **2011**, *3*, 1120–1126.
- (21) Hu, G. C.; Shan, C. X.; Zhang, N.; Jiang, M. M.; Wang, S. P.; Shen, D. Z. High Gain Ga<sub>2</sub>O<sub>3</sub> Solar-Blind Photodetectors Realized via a Carrier Multiplication Process. *Opt. Express* **2015**, *23*, 13554–13561.
- (22) Yu, F. P.; Ou, S. L.; Wu, D. S. Pulsed Laser Deposition of Gallium Oxide Films for High Performance Solar-Blind Photodetectors. *Opt. Mater. Express* **2015**, *5*, 1240–1249.
- (23) Guo, D. Y.; Wu, Z. P.; Li, P. G.; An, Y. H.; Liu, H.; Guo, X. C.; Yan, H.; Wang, G. F.; Sun, C. L.; Li, L. H.; Tang, W. H. Fabrication of Beta-Ga<sub>2</sub>O<sub>3</sub> Thin Films and Solar-Blind Photodetectors by Laser MBE Technology. *Opt. Mater. Express* **2014**, *4*, 1067–1076.
- (24) Suzuki, R.; Nakagomi, S.; Kokubun, Y.; Arai, N.; Ohira, S. Enhancement of Responsivity in Solar-Blind Beta-Ga<sub>2</sub>O<sub>3</sub> Photodiodes with a Au Schottky Contact Fabricated on Single Crystal Substrates by Annealing. *Appl. Phys. Lett.* **2009**, *94*, 222102-1–222102-3.
- (25) Suzuki, R.; Nakagomi, S.; Kokubun, Y. Solar-Blind Photodiodes Composed of a Au Schottky Contact and a Beta-Ga<sub>2</sub>O<sub>3</sub> Single Crystal with a High Resistivity Cap Layer. *Appl. Phys. Lett.* **2011**, *98*, 131114-1–131114-3.
- (26) Tian, W.; Zhi, C. Y.; Zhai, T. Y.; Chen, S. M.; Wang, X.; Liao, M. Y.; Golberg, D.; Bando, Y. In-Doped Ga<sub>2</sub>O<sub>3</sub> Nanobelt Based Photodetector with High Sensitivity and Wide-Range Photoresponse. *J. Mater. Chem.* **2012**, *22*, 17984–17991.
- (27) Zou, R. J.; Zhang, Z. Y.; Liu, Q.; Hu, J. Q.; Sang, L. W.; Liao, M. Y.; Zhang, W. J. High Detectivity Solar-Blind High-Temperature Deep-Ultraviolet Photodetector Based on Multi-Layered (100) Facet-Oriented beta-Ga<sub>2</sub>O<sub>3</sub> Nanobelts. *Small* **2014**, *10*, 1848–1856.
- (28) Weng, W. Y.; Hsueh, T. J.; Chang, S. J.; Huang, G. J.; Hung, S. C. Growth of Ga<sub>2</sub>O<sub>3</sub> Nanowires and the Fabrication of Solar-Blind Photodetector. *IEEE Trans. Nanotechnol.* **2011**, *10*, 1047–1052.
- (29) Guo, D. Y.; Wu, Z. P.; Li, P. G.; Wang, Q. J.; Lei, M.; Li, L. H.; Tang, W. H. Magnetic Anisotropy and Deep Ultraviolet Photo-response Characteristics in Ga<sub>2</sub>O<sub>3</sub>: Cr Vermicular Nanowire Thin Film Nanostructure. *RSC Adv.* **2015**, *5*, 12894–12898.
- (30) Nakamura, S.; Mukai, T.; Senoh, M. Candela-Class High-Brightness InGaN/AlGaIn Double-Heterostructure Blue-Light-Emitting Diodes. *Appl. Phys. Lett.* **1994**, *64*, 1687–1689.
- (31) Passlack, M.; Schubert, E. F.; Hobson, W. S.; Hong, M.; Moriya, N.; Chu, S. N. G.; Konstadimidis, K.; Mannaerts, J. P.; Schnoes, M. L.; Zydzik, G. J. Ga<sub>2</sub>O<sub>3</sub> Films For Electronic and Optoelectronic Applications. *J. Appl. Phys.* **1995**, *77*, 686–693.
- (32) Konstantatos, G.; Howard, I.; Fischer, A.; Hoogland, S.; Clifford, J.; Klem, E.; Levina, L.; Sargent, E. H. Ultrasensitive Solution-Cast Quantum Dot Photodetectors. *Nature* **2006**, *442*, 180–183.
- (33) Wang, X.; Tian, W.; Liao, M. Y.; Bando, Y.; Golberg, D. Recent Advances in Solution-Processed Inorganic Nanofilm Photodetectors. *Chem. Soc. Rev.* **2014**, *43*, 1400–1422.
- (34) Roderick, E. H.; Williams, R. H. *Metal Semiconductor Contacts*, 2nd ed; Clarendon: Oxford, 1988.
- (35) Wen, L. Y.; Wong, K. M.; Fang, Y. G.; Wu, M. H.; Lei, Y. Fabrication and Characterization of Well-Aligned, High Density ZnO Nanowire Arrays and Their Realizations in Schottky Device Applications Using a Two-Step Approach. *J. Mater. Chem.* **2011**, *21*, 7090–7097.
- (36) Harnack, O.; Pacholski, C.; Weller, H.; Yasuda, A.; Wessels, J. M. Rectifying Behavior of Electrically Aligned ZnO Nanorods. *Nano Lett.* **2003**, *3*, 1097–1101.
- (37) Liu, K. W.; Sakurai, M.; Aono, M. Controlling Semiconducting and Insulating States of SnO<sub>2</sub> Reversibly by Stress and Voltage. *ACS Nano* **2012**, *6*, 7209–7215.
- (38) Liu, K. W.; Sakurai, M.; Aono, M. Enhancing the Humidity Sensitivity of Ga<sub>2</sub>O<sub>3</sub>/SnO<sub>2</sub> Core/Shell Microribbon by Applying Mechanical Strain and Its Application as a Flexible Strain Sensor. *Small* **2012**, *8*, 3599–3604.
- (39) Taguchi, A.; Saito, Y.; Watanabe, K.; Yijian, S.; Kawata, S. Tailoring Plasmon Resonances in the Deep-Ultraviolet by Size-Tunable Fabrication of Aluminum Nanostructures. *Appl. Phys. Lett.* **2012**, *101*, 081110-1–081110-4.
- (40) Chen, H. Y.; Liu, K. W.; Jiang, M. M.; Zhang, Z. Z.; Xie, X. H.; Wang, D. K.; Liu, L.; Li, B. H.; Zhao, D. X.; Shan, C. X.; Shen, D. Z. Tunable Enhancement of Exciton Emission from MgZnO by Hybridized Quadrupole Plasmons in Ag Nanoparticle Aggregation. *Appl. Phys. Lett.* **2014**, *104*, 091119-1–091119-4.
- (41) Gao, N.; Huang, K.; Li, J. C.; Li, S. P.; Yang, X.; Kang, J. Y. Surface-Plasmon-Enhanced Deep-UV Light Emitting Diodes Based on AlGaIn Multi-Quantum Wells. *Sci. Rep.* **2012**, *2*, 816-1–816-6.